HOSTED BY
ELSEVIER

Contents lists available at ScienceDirect

Asian Pacific Journal of Tropical Medicine

journal homepage: http://ees.elsevier.com/apjtm

Original research http://dx.doi.org/10.1016/j.apjtm.2016.06.008

Insight of ZnS nanoparticles contribution in different biological uses

Houcine Labiadh[1*], Karima Lahbib[2], Slah Hidouri[3], Soufiane Touil[2], Tahar BEN Chaabane[1]

[1]*Unité de Recherche UR11ES30 de Synthèse et Structures de Nanomatériaux, Faculté des Sciences de Bizerte, 7021 Jarzouna, Tunisia*

[2]*Laboratory of Heteroatom Organic Chemistry, Department of Chemistry, Faculty of Sciences of Bizerte, Carthage University, 7021 Jarzouna, Tunisia*

[3]*Department of Research in Sciences of Life and Materials, Faculty of Sciences of Bizerte, Carthage University, Tunisia*

ARTICLE INFO

Article history:
Received 15 May 2016
Received in revised form 16 Jun 2016
Accepted 21 Jun 2016
Available online 29 Jun 2016

Keywords:
Nanoparticles
Semiconductors
Antioxidant activity
Antibacterial activity
Antifungal activity

ABSTRACT

Objectives: To evaluate the contributions of the some quantum dots in different biological uses in order to valorizes such nanomaterials for further applications.

Methods: Zinc sulfide ZnS nanoparticles were synthesized in aqueous medium at pH constant, the obtained nanoparticles has been characterized by X-ray diffraction (XRD), transmission electron microscopy (TEM) and Fourier Transform Infra-red (FTIR) spectroscopies. Zinc sulfide nanoparticles were screened for their antibacterial and antifungal profiling and tested for antioxidant activity using 1,1-diphenyl-2-picrylhydrazyl (DPPH), hydroxyl radical ($OH^{\bullet}$) and hydrogen peroxide (H_2O_2) scavenging activity, ferric reducing power (FRP) assay and ferrous ion chelating (FIC) methods.

Results: The sizes of the crystallites were estimated to 3 nm using the Debye-Scherrer formula based on the XRD data. The shape was identified to be quasi-spherical with agglomerated particles. The obtained ZnS quantum dots present an antioxidant activity especially in oxido-reduction power, and can be used for species profiling either for bacteria and fungus.

Conclusion: It was found that ZnS nanoparticles showed relatively higher antioxidant activities and antibacterial with an antifungal behavior which proves that this nanomaterials can react at the interface with the life entities.

1. Introduction

Synthesis of nanoparticles has been given a great attention in synthesis engineering and phase combination design. Among various classes of nanoparticles, semiconductor nanomaterials have emerged as important materials with promising applications such as in nanotechnology and biology applications [1–6]. For instance, many methods have been used to synthesize ZnS nanostructures for specific use in biological detection and tagging molecules [7]. Therefore, ZnS nanoparticles are characterized by their attractive proprieties which participate for restricted area of application especially pharmaceutics uses [8,9]. Various engineered nanoparticles have become important tools in biomedical research in addition to the optical use in live-cell imaging and *in vivo* diagnostic imaging [10–22]. Despite advantages of nanoparticles, the toxicity has been thoroughly examined, it was revealed that it is mainly attributed to the toxic effects of metals leaching from the nanoparticles or derived from their intrinsic properties such as size and roughness of the surface.

In this context, the present study was focused on the contribution of ZnS nanoparticles in biological uses, for that, nanoparticles has been synthesized and structurally characterized before been used in the *in vitro* evaluation of their antioxidant activities using 1,1-diphenyl-2-picrylhydrazyl (DPPH), hydroxyl radical ($OH^{\bullet}$) scavenging activity, ferric reducing power (FRP) assay and ferrous ion chelating (FIC). The study has been reinforced by screening *in vivo* tests for inactivation profiling with bacteria and fungus selected species.

2. Material and methods

2.1. Synthesis of ZnS nanoparticles

ZnS nanoparticles were prepared in aqueous medium regarding the protocol using equimolar (25 mL, 0.5 M) mixture of zinc acetate and thioacetamide under continuous magnetic

*Corresponding author: Houcine Labiadh, UR11ES30 of Synthesis and Structure of Nanomaterials, Department of Chemistry, Faculty of Sciences of Bizerta, Carthage University, 7021 Jarzouna, Tunisia.
E-mail: labiadhhoucine1983@gmail.com

Peer review under responsibility of Hainan Medical College.

stirring. The mixture was then heated for 3 h at 85 °C. After cooling to room temperature, the powder was collected by centrifugation, washed several times with absolute ethanol and dried for 12 h at 60 °C.

2.2. Structural characterization

The structure of the crystalline phase of the as-synthesized powders was characterized by X-ray diffraction (XRD) on a BRUKER D8 ADVANCE diffractometer using Cu Kα radiation.

FTIR spectrum has been performed by a Nicolet UR 200 FT-IR spectrometer with ATR mode the spectrum has been recorded over the 400–4 000 cm^{-1} range. The particles morphology study was carried out using FEI Tecnai G2 Transmission Electron Microscope (TEM) operating at 200 kV. Spectrophotometry analyses were performed using an UV spectrophotometer (6005).

2.3. Antioxidant evaluation

Antioxidant activities has been revealed *in vitro* tests for DPPH Radical Scavenging Activity [23], Hydroxyl Radical Scavenging Activity [24,25], Hydrogen peroxide scavenging activity [26] and Reducing Power Assay [27] either Ferrous ion chelating ability (FIC) [28], the details of the experiment has been performed as mention by Lahbib *et al.* [29] with all details for statistic calculation of IC_{50} (the concentration of test product required for 50% of inhibition).

2.4. Biolog phenotype microarray tests

2.4.1. Biolog phenotype microarray technology

The phenotype analysis was carried out by using a new tool, Phenotype Micro Arrays (PMs). Biolog's Phenotype Micro Array technology (Biolog, USA) offers a unique way to identify product and to infer a mode of action by which the novel inhibitor prevents microbial growth [30]. The assays are pre-filled and dried in 96-well microplates that can monitor chemical sensitivities. Cell response in each assay well is determined by the amount of color development produced by the reduction of a tetrazolium compound (a redox indicator) during cell respiration [31]. To identify the method of action of compounds on Gram negative and Gram positive bacteria, PMs were employed to screen various sources of carbon, nitrogen, sulfur and phosphorous. The methods were done according to the PM procedure for *Enterococcus coli* (*E. coli*) and other Gram negative bacteria and the PM procedure for *Bacillus subtilis* (*B. subtilis*) and other Gram positive bacteria provided by Biolog Inc., USA. All the fluids, PMs, and instruments were purchased from Biolog Inc., USA. Kinetic data were analyzed with OmniLog PM software (Biolog, USA). The results were expressed by the differences of the treated bacterial cells from untreated bacterial cells (control group).

2.4.2. PMs of ZnS with bacteria

E. coli (ATCC 8739), *Enterococcus faecalis* (*E. faecalis*, *Ec P07*) and *B. subtilis* was grown overnight at 37 °C on nutrient agar plates. In order to prepare the bacteria cell suspension, colonies were harvested from the surface of an agar plate with a sterile cotton wool swab and suspended in 16 mL of Inoculating Tryptic Soy Broth (TSB), in a 20 mL sterile capped glass tube. The cell density must be equaled to 80%–85% transmittance on a Biolog turbidimeter. The TSB with Biolog Redox Dye Mix was also prepared. Later, 250 μL/well were added to PM plates in details 100 μL/well from bacteria suspension, 130 μL/well of TSB with Biolog Redox Dye Mix correspondent and 20 μL/well of ZnS solution (at different concentration from 0.001 to 0.1 mg/mL). All the plates were incubated at 37 °C in the OmniLog plate, results were recorded after 48 h for all PM plates.

2.4.3. PMs of ZnS with fungus

Alternaria alternate (*A. alternate*) and *Fusarium solani* (*F. solani*) were grown on nutrient agar plates overnight at 37 °C. In order to prepare the fungi cell suspension, colonies were harvested from the surface of an agar plate with a sterile cotton wool swab and suspended in 16 mL of Inoculating Malt extract in a 20 mL sterile capped glass tube. The cell density must be equaled to 62% transmittance on a Biolog turbidimeter. The ME with Biolog Redox Dye Mix F was also prepared. Later, 250 μL/well using Biolog multichannel pipette were added to PM plates in detail, 20 μL/well fungi cell suspension, 210 μL/well ME with Biolog Redox Dye Mix F and finally 20 μL/well ZnS was added respecting the concentrations tested. All the plates were incubated at 37 °C in the OmniLog plate incubator and reader and were monitored for any color change of the wells. Readings were recorded for 48 h for all PM plates.

2.5. Bacterial inactivation study

E. coli samples stain *E. coli* K12 (Deutsche Sammlung von Mikroorganismen und ZellkulturenFig GmbH (DSMZ) ATCC237 16, Braunschweig, Germany) were used for the ZnS antibacterial activity like described by Petronella [32]. The polyester fabrics were sterilized by autoclaving at 121 °C for 2 h. Three independent assays were performed for the sputtered textile sample. The solar simulated light source has been done by a solar simulator (Heraeus, Hannau, Germany) with a light emission between 200 and 800 nm provided for a 100 W Xe-light resembling to the solar spectrum with a light intensity of 50 mW/cm^2.

3. Results

3.1. Structural characterizations

3.1.1. XRD profile of synthesized ZnS

The wide angle XRD patterns of ZnS nanocrystals exhibit the (111), (220), and (311) planes as given in Figure 1, that shows the cubic zinc blend phase according to pdf sheet JCPDS. no 05-0566. The broadness of the peaks is due to the small size of the crystals. No diffraction peaks from impurities was detected in the sample. To better explore the XRD profile, the diameter of ZnS particles have been estimated using Debye-Scherrer formula [33]:

$$L = 0.9\lambda/\beta \cos\theta \quad (1)$$

Where β is the full width at half maximum (FWHM) of the diffraction peak in radians, θ is Bragg's diffraction angle and λ is the wavelength for the $K\alpha_1$ component of the copper radiation employed (1.5418 Å). The average size of the ZnS crystallites was found to be around 3 nm.

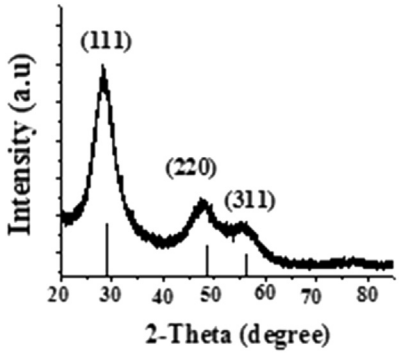

Figure 1. XRD patterns of ZnS particle.

3.1.2. TEM micrograph

TEM image of the ZnS particles is given in Figure 2, which shows almost a spherical aggregates constituted by nanometer-sized crystals. The aggregation observed is probably due to S−S bridges that can be formed between sulfide particles [34].

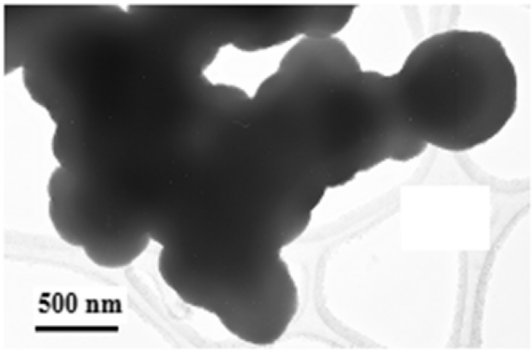

Figure 2. TEM images of ZnS nanoparticles for 3 h at 85 °C.

3.2. Raman spectra

The Raman spectrum recorded in the frequency range 200–450 cm^{-1} display strong peaks at ~265 and 347 cm^{-1} the details are given in Figure 3. Brafman and Mitra [35] have reported Raman spectra of bulk hexagonal and cubic phases of ZnS, they observed TO and LO zone center phonons of cubic ZnS crystals at 276 and 351 cm^{-1}, respectively, and the E_2 modes of wurtzite ZnS at 72 and 286 cm^{-1}. The absence of peaks at 72 and 286 cm^{-1} in the Raman spectra in case of ZnS samples confirmed the cubic crystalline system of the compound.

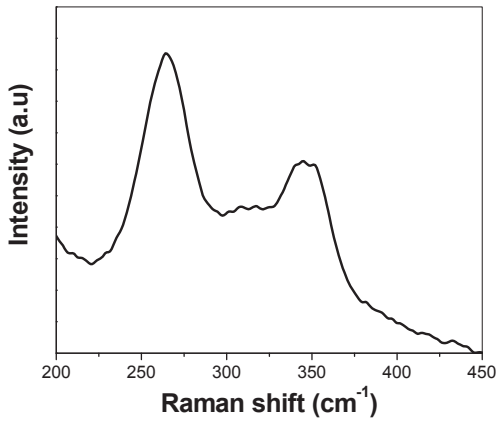

Figure 3. Raman spectra of ZnS nanoparticle.

3.3. Infrared manifestation of the ZnS

Infrared spectrum of synthesized ZnS nanoparticles is given in Figure 4. It shows different characteristic peaks, the broad absorption band centered at 3 200 cm^{-1} can be attributed to O−H stretching mode of H_2O adsorbed on the surface of the particles. The two bands observed at 1 560 and 1 428 cm^{-1} are due to the asymmetrical and symmetrical stretching of the zinc carboxylate (COO^-) respectively [36]. The peak situated around 1 037 cm^{-1} may be attributed to S−O stretching and the one that appearing at 678 cm^{-1} is characteristic of the ZnS stretching vibration [37].

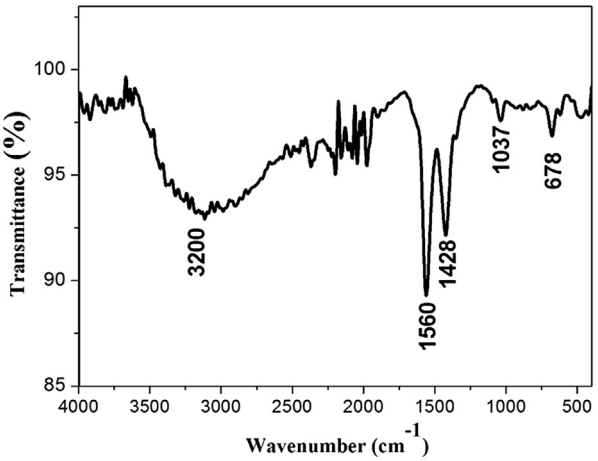

Figure 4. FT-IR spectra of ZnS nanoparticles.

3.4. Biological phenotypage analysis

The investigation of microorganisms profiling of the synthesized nanomaterial regarding three bacteria strain and tow species of fungus present a results given in Table 1 which showed a high antibacterial activity compared to absolute ethanol with an IC_{50} at around 0.001 mg/mL both for *E. faecalis* and *B. subtilis*, whereas, *E. coli* has been more resistant to the effect of ZnS nanoparticles with an IC $_{50}$ at 0.7 36 mg/mL. The antifungal activity compared with absolute ethanol has been evaluated to an IC_{50} at around 0.01 mg/mL for the tow tested species *A. alternate* and *F. solani*.

The resistance behavior of *E. coli* has been revealed in this test and explains that at the condition of the experiment, these bacteria can grow normally, as the ZnS optic proprieties can be induced and manipulated when the particles absorb a sufficient light energy, a test of inhibition after exposition of the treated bacteria to the solar like light has been carried out. A preliminary exploration of emission propriety of the ZnS in biological application can be used in order to look for the bacterial inactivation consequences under ordinary light that can be done in quotidian life; Figure 5 shows the results the simulated solar light of 50 mW/cm^2 was applied to the exposed *E. coli* by ZnS nanoparticles. ZnS did not induce bacterial inactivation in a short period of time but after 240 min of treatment lead the inactivation. In evidence mention that ZnS can be used for antiseptic uses under solar light.

3.5. Antioxidant proprieties of ZnS

In order to estimate the effect of ZnS nanoparticles on antioxidant system, *in vitro* tests have been carried respecting

Table 1
Antibacterial and antifungal activities of ZnS nanoparticles.

	E. coli (ATCC 8739)	*E. faecalis* (Ec P07)	*B. subtilis*	*A. alternata*	*F. solani*
Ethanol 95% (%)	11.33	61.02	45.51	37.22	35.90
ZnS (IC_{50} mg/mL)	0.736 ± 0.070	0.0 010 ± 0.000	0.0 012 ± 0.0001	0.009 ± 0.0 006	0.012 ± 0.001

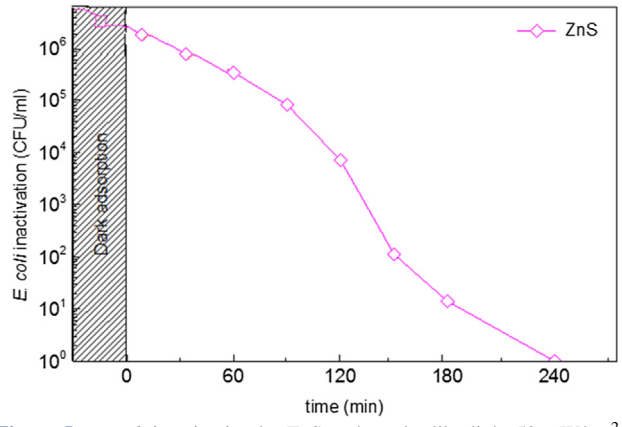

Figure 5. *E. coli* inactivation by ZnS under solar-like light 50 mW/cm^2.

different level in the above mentioned system, results are summarized in Figure 6. ZnS nanoparticles show a DPPH radical scavenging activity with an IC_{50} at 6.61 ± 0.31 mg/mL which is more than 10 times compared to ascorbic acid (IC_{50}: 0.0396 ± 0.002 mg/mL), which can be explained by a limited power of the ZnS phase to cede a requested proton to reduce the DPPH. Regarding the FTIR profile of the nanomaterials the particles do not contain protons at the surface it is only water molecule that gain the surface.

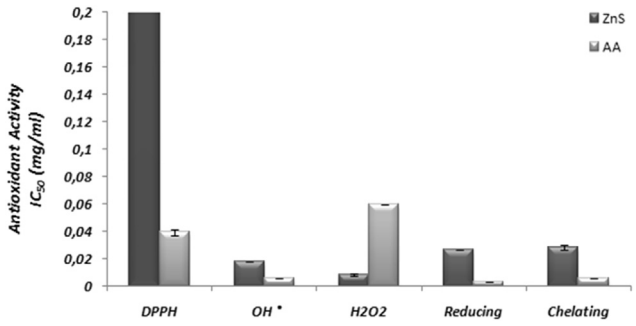

Figure 6. Antioxidant activity.

In case of test for a possible ability to collect proton from the reaction medium, ZnS particle has an OH$^•$ radical scavenging activity near to the AA, IC_{50} (ZnS) was at 0.017 ± 0.0001 mg/mL compared to ascorbic acid (IC_{50}: 0.006 ± 0.00001 mg/mL) which can be considered as a propriety of the present compound and show the existence of probable sites that collect hydroxyl.

Hydrogen peroxide test present a higher scavenging activity of ZnS with IC_{50} at 0.0084 ± 0.0009 mg/mL which allow it usage in this restricted test however the value for the standard compound the AA present an IC_{50}: 0.06 ± 0.00001 mg/mL.

The behavior of the ZnS synthesized nanoparticles has been tested for its capacity to cede either to collect electron from the oxydoreduction reaction carried by iron, results show that ZnS particle showed a good reducing power with IC_{50} at 0.026 ± 0.0001 mg/mL compared to ascorbic acid (IC_{50}: 0.0035 ± 0.00004 mg/mL). This is a synonym of the ability to cede an electron for the reactional medium when it is required. The oxidation power has been evaluated to be at high level of ferrous ion chelating ability with IC_{50} at 0.028 ± 0.0019 mg/mL compared to the ascorbic acid (IC_{50}: 0.0057 ± 0.0002 mg/mL).

Results are expressed as mean ± SEM (n = 3).

4. Discussion

This study described the efficiency of ZnS as antibacterial, antifungal and antioxidant agent. First, the antibacterial effects under simulated solar light of 50 mW/cm^2 tested with *E. coli* bacteria were outlined, the stimulation of ZnS by ordinary light switch the effect regarding the preliminary resistant strain *E. coli* which present a novel exploration of the antibacterial effect using ZnS by light stimulated conditions to get better result and explain the contribution of the optic propriety in the restricted application. Whereas ZnS exhibited an antibacterial activity without any supplementary activation with *E. faecalis* and *B. subtilis*, the same result has been observed with the two tested fungi *Alternaria alternate* and *Fusarium solani*. This findings are in agreement with those obtained by Azm *et al.*, showing that undoped nanoparticles could increase ROS generation [9] and are responsible for stop bacteria bacteria through chemical phenomena [9,38]. Regarding the mechanism of action, it is important to mention that inactivation power of nanoparticles could be explained by the capacity of transporting charge carriers to the surface of the nanoparticles via defect levels in the forbidden gap which make possibility of interaction with oxygen and water molecules to generate more ROS [9]. Moreover, since nanoparticles are efficient energy donors [39,40], they could transfer energy to nearby oxygen molecules inducing the generation of reactive oxygen species (ROS) and in turn leading to cell damage or death [41].

In the second part of this work, the study focused on the *in vitro* antioxidant effect of the ZnS particles, results showed that ZnS exhibited a possible antioxidant activity referring to ascorbic acid. This indicate that ZnS nanocrystals have a higher OH$^•$ and H_2O_2 scavenging activities more than DPPH. These results were relatively confirmed by the experiment done by Rakcha *et al.*, which show that commercial undoped ZnS is more OH$^•$ scavenging than doped ZnS [42]. This evidence show that undoped ZnS have an efficient direct antioxidant when the OH$^•$ scavenging activity predominates over OH$^•$ generation. These results were in agreement with those performed by Seung Soo [43], who suggested that nanoparticles have the ability to absorb and release oxygen ions in a chemical reaction known as reduction-oxidation reaction. When ROS increase, nanoparticles react immediately in order to absorb free radicals [43]. In the first state, nanoparticles have sufficient gaps energy in their surface that makes possible absorption of oxygen ions like a sponge. In addition, when nanoparticles are mixed with free radicals, they catalyze a reaction that effectively defangs the ROS by capturing oxygen atoms; the particles

then slowly release their captured oxygen and can break down free radicals again [40]. These results were further confirmed by the high undoped ZnS activity as chelating and reducing power. These results suggest that ZnS could be considered as a chelator and also as a secondary antioxidant by inhibiting the Fenton reaction. In these reactions, iron plays an important role suggesting that the selective *in vitro* antioxidant properties of the nanoparticles are due to their iron chelating characteristics. Recently, nanoparticles have been proven to prevent Alzheimer disease, progressing Alzheimer disease and other neurologic disorders associated with trace metal imbalance.

The results presented highlight the possible uses of ZnS nanoparticles in different biological level of study. The right crystalline phase of ZnS with a particular size present a multi-capacity for antioxidant intervention either for generation of electrons that can be released in the reactional medium to serve as reducing agent when the electron has been in demand or an oxidizer agent to accomplish oxydo-reduction reaction, this ability have been evidenced by the *in vitro* tests. Regarding the hydroxides species the ZnS nanoparticles can reside the hydroxyl anion from the aqueous solution however regarding the poorly modified surface as revealed by FTIR analysis it has a limited ability to generate proton when requested in case DPPH reducing ability. Finally, the ZnS nanoparticles have been used for species profiling regarding the ability to act as antibacterial or antifungal agent.

Conflict of interest statement

The authors declare that there is no conflict of interest regarding the publication of this document.

References

[1] Radhu S, Vijayan C. Observation of redemission in wurtzite ZnS nanoparticles and the in vestigation of phononmo des by Raman spectroscopy. *Mater Chem Phys* 2011; **129**: 1132-1137.

[2] Fang SX, Zhai TY, Gautam UK, Li L, Wu LM. ZnS nanostructures: from synthesis to applications. *Prog Mater Sci* 2011; **56**: 275-287.

[3] Kaur Gurvir, Tripathi SK. Size tuning of MAA capped CdSe and CdSe/CdS quantum dots and their stability in different pH environments. *Mater Chem Phys* 2014; **143**: 514-523.

[4] Li Zhenshun, Xu Wei, Yuntao W, Bakht RS, Chunlan ZH, Yijie C, et al. Quantum dots loaded nanogels for low cytotoxicity, pH-sensitive fluorescence, cell imaging and drug delivery. *Carbohyd Polym* 2015; **121**: 477-485.

[5] Valentina VG, Vladislav AP, Alexey VM, Dries VG, Sarah DS, Goryacheva Irina Yu. Hydrophilic quantum dots stability against an external low-strength electric field. *Apply Surf Sci* 2016; **363**: 259-263.

[6] Yuan RG, Hui J, Zonghua W, Lianjiang T. Recent advances in synthetic methods and applications of colloidal silver chalcogenide quantum dots. *Coord Chem Rev* 2015; **296**: 91-124.

[7] Qing J, Li Yan, Jianzhong H, Xiaojun Z. The "off–on" phosphorescent switch of Mn-doped ZnS quantum dots for detection of glutathione in food, wine, and biological samples. *Sens Actuat B* 2016; **227**: 108-116.

[8] Kavitha P, Huey-Min H, Xu Hong, Zoraida PA, Andrew W. *In vitro* cytotoxicity of CdSe/ZnS quantum dots with different surface coatings to human keratinocytes HaCaT cells. *J Environ Sci* 2013; **25**(1): 163-171.

[9] Rakshaa KR, Anandab S, Madegowda NM. Netkal MMa. Study of kinetics of photocatalysis, bacterial inactivation and $OH^{\bullet}$ scavenging activity of electrochemically synthesized Se^{4+} doped ZnS nanoparticles. *J Mol Catal A Chem* 2015; **396**: 319-327.

[10] Zhu ZJ, Yeh YC, Tang R, Yan B, Tamayo J, Vachet RW, et al. Stability of quantum dots in live cells. *Nat Chem* 2011; **3**: 963-968.

[11] Yi Zhang, Wang T. Quantum dot enabled molecular sensing and diagnostics. *Theranostics* 2012; **2**(7): 631-654.

[12] Daniel SL, William SP, Ken HL, Mark H, Alice YT. Quantum dot targeting with lipoic acid ligase and halotag for single molecule imaging on living cells. *ACS Nano* 2012; **6**(12): 11080-11087.

[13] Gonda K, Miyashita M, Higuchi H, Tada H, Watanabe TM, Watanabe M, et al. Predictive diagnosis of the risk of breast cancer recurrence after surgery by single-particle quantum dot imaging. *Aca J* 2015; **14**: 322.

[14] Mariana T, Manish KS, Emerson G, Alexandra F, Vincent L, Marie R, et al. Oriented bioconjugation of unmodified antibodies to quantum dots capped with copolymeric ligands as versatile cellular imaging tools. *ACS Appl Mater Inter* 2015; **7**(48): 26904-26913.

[15] Paolo P, Giovanni C. Quantum dots to tail single bio-molecules inside living cells. *Adva Dru Deliv Rev* 2012; **64**: 167-178.

[16] Min F, Chun WP, Dai WP, Li Yan. Quantum dots for cancer research: current status, remaining issues, and future perspectives. *Cancer Biol Med* 2012; **9**(3): 151-163.

[17] Yuri V. Quantum dots in nanomedicine: recent trends, advances and unresolved issues. *Biochem Biophys Res Commun* 2015; **468**: 419-427.

[18] König K, Raphael AP, Lin L, Grice JE, Soyer HP, Breunig HG, et al. Applications of multiphoton tomographs and femtosecond laser nanoprocessing microscopes in drug delivery research. *Advan Drug Deliv Rev* 2011; **63**: 388-400.

[19] Vivek KP, Yuvraj S, Jaya GM, Siddharth G, Manish K Ch. Engineered nanocrystal technology: in-vivo fate, targeting and applications in drug delivery. *J Control Release* 2014; **183**: 51-66.

[20] Qiong W, Chen L, Liang H, Jing W, Jiawei L, Chao H, et al. Quantum dots decorated gold nanorod as fluorescent-plasmonic dualmodal contrasts agent for cancer imaging. *Biosens Bioelectron* 2015; **74**: 16-23.

[21] Xiaoyuan J, Fei P, Yiling Z, Yuanyuan Su, Yao He. Fluorescent quantum dots: synthesis, biomedical optical imaging, and biosafety assessment. *Colloids Surf B Bio Interfaces* 2014; **124**: 132-139.

[22] Jutaek N, Nayoun W, Jiwon B, Jin Ho, Joonhyuck P, Sungwook J, et al. Surface engineering of inorganic nanoparticles for imaging and therapy. *Adv Drug Deliv Rev* 2013; **65**: 622-648.

[23] Sangeetha R, Muthukumaran S, Ashokkumar M. Structural, optical, dielectric and antibacterial studies of Mn doped $Zn_{0.96}Cu_{0.04}O$ nanoparticles. *Spectrochim Acta A Mol Biomol Spectrosc* 2015; **144**: 1-7.

[24] Burcu B, Mustafa Z, Kubilay G, Resat A. Novel spectroscopic sensor for the hydroxyl radical scavenging activity measurement of biological samples. *Talanta* 2012; **99**: 689-696.

[25] Hadi G, Behrouz JG, Prakash HS. Hepatoprotective and cytoprotective properties of Hyptis suaveolens against oxidative stress-induced damage by CCl_4 and H_2O_2. *Asia Pac J Trop Med* 2012; **5**(11): 868-874.

[26] Ali A, Touseef AW, Idrees AW, Farooq AM. Comparative study of the physico-chemical properties of rice and corn starches grown in Indian temperate climate. *J Saudi Soc Agric Sci* 2016; **15**: 75-82.

[27] Vivek KB, Ajay S, Sun Ch K, Kwang HB. Antioxidant, lipid peroxidation inhibition and free radical scavenging efficacy of a diterpenoid compound sugiol isolated from *Metasequoia glyptostroboides*. *Asian Pac J Trop Med* 2014; **1**: 9-15.

[28] Hossain MA, Muhammad DS, Charles G, Muhammad I. *In vitro* total phenolics, flavonoids contents and antioxidant activity of essential oil, various organic extracts from the leaves of tropical medicinal plant Tetrastigma from Sabah. *Asian Pac J Trop Med* 2011; **9**: 717-721.

[29] Karima L, Mohamed T, Soufiane T. Evaluation of net antioxidant activity of mono- and bis-Mannich base hydrochlorides and 3-keto-1,5-bisphosphonates from their ProAntidex parameter. *J Mol Stru* 2015; **1091**: 152-158.

[30] Sharon B, Dominique J, Kristen MD, Jane K, Patrik D, Marcin PJ, et al. Application of phenotypic microarrays to environmental microbiology. *Curr Opin Biotechnol* 2012; **23**: 41-48.
[31] Hurlemann R, Dirk Sc. Dissecting the role of oxytocin in the formation and loss of social relationships. *Biol Psychiat* 2016; **79**: 185-193.
[32] Rtimi S, Baghriche O, Sanjines R, Pulgarin C, Bensimon M, Kiwi J. TiON and TiON-Ag sputtered surfaces leading to bacterial inactivation under indooractinic light. *J Photochem Photobiol A Chem* 2013; **256**: 52-63.
[33] Zhang Yue, Meiyan Yu. One pot synthesis and characterization of ZnS nanoparticles in the mixed surfactant system. *Mater Chem Phys* 2014; **145**: 197-202.
[34] Tahar A, Houcine L, Gaceur M, Montero D, Ammar S, Smiri L, et al. Structural, microstructural and optical characterization of polyol-mediated ZnS/PVP nanocomposite powders and films. *J Mater Environ Sci* 2012; **3**: 1147-1152.
[35] Anthony A, Collins N. *In vitro* properties of surface modified solid lipid microspheres containing an antimalarial drug: halofantrine. *Asian Pac J Trop Med* 2011; **4**: 253-258.
[36] Basti H, Ben Tahar L, Smiri LS, Herbest F, Vaulay MJ, Chau F, et al. Catechol derivatives-coated Fe_3O_4 and γ-Fe_2O_3 nanoparticles as potential MRI contrast agents. *J Colloid Interface Sci* 2010; **341**: 248-254.
[37] Mubashshir M, Farooqi H, Srivastava K. Structural, optical and photoconductivity study of ZnS nanoparticles synthesized by a low temperature solid state reaction method. *Mat Sci Semicon Proc* 2014; **20**: 61-67.
[38] Seung Soo L, Wensi S, Minjung C, Hema LP, Phuc N, Huiguang Z, et al. Antioxidant properties of cerium oxide nanocrystals as a function of nanocrystal diameter and surface coating. *ACS Nano* 2013; **7**(11): 9693-9703.
[39] Azam A, Ahmed AS, Oves M, Khan MS, Habib SS, Memic A. Antimicrobial activity of metal oxide nanoparticles against gram-positive and gram-negative bacteria: a comparative study. *Int J Nanomed* 2012; **7**: 6003-6009.
[40] Labiadh H, Ben Chaabane T, Balanb L, Becheik N, Corbel S, Medjahdid G, et al. Preparation of Cu-doped ZnS QDs/TiO_2 nanocomposites with high photocatalytic activity. *Appl Catal B Envir* 2014; **144**: 29-35.
[41] Kwang SA, Kyung RL, Daeho J, Bo Young Lee, Kwan SK, Won YL. Fluorescence energy transfer inhibition bioassay for cholera toxin based on galactose-stabilized gold nanoparticles and amine-terminated quantum dots. *Micr Chem J* 2016; **124**: 9-14.
[42] Jing W, Hai B, Zhangfa T, ChangSik H. Fluorescent/luminescent detection of natural amino acids by organometallic systems. *Coord Chem Rev* 2015; **303**: 139-184.
[43] Michael J, Leon F, Leticia G. Using computational chemistry to design Ru photosensitizers with directional charge transfer. *Coord Chem Rev* 2015; **304**: 146-165.